Tuning Hydrophobicity and Water Adhesion by Electrospinning and Silanization

ARTICLE *in* LANGMUIR · MARCH 2011

Impact Factor: 4.46 · DOI: 10.1021/la104978e · Source: PubMed

5 AUTHORS, INCLUDING:

Thanarath Pisuchpen
Chulalongkorn University
2 PUBLICATIONS **21** CITATIONS
SEE PROFILE

Pitt Supaphol
Chulalongkorn University
234 PUBLICATIONS **6,463** CITATIONS
SEE PROFILE

Voravee P Hoven
Chulalongkorn University
31 PUBLICATIONS **518** CITATIONS
SEE PROFILE

Langmuir

ARTICLE

pubs.acs.org/Langmuir

Tuning Hydrophobicity and Water Adhesion by Electrospinning and Silanization

Thanarath Pisuchpen,[†] Navarun Chaim-ngoen,[‡,§] Narupol Intasanta,[∥] Pitt Supaphol,[§,⊥] and Voravee P. Hoven[*,†]

[†]Organic Synthesis Research Unit, Department of Chemistry, Faculty of Science, [‡]Program in Petrochemistry and Polymer Science, Faculty of Science, [§]Center for Petroleum, Petrochemicals, and Advanced Materials, and [⊥]Petroleum and Petrochemical College, Chulalongkorn University, Phayathai Road, Pathumwan, Bangkok 10330, Thailand

[∥]National Nanotechnology Center, National Science and Technology Development Agency, Thailand Science Park, Phahonyothin Road, Klong Luang, Pathumthani 12120, Thailand

ABSTRACT:

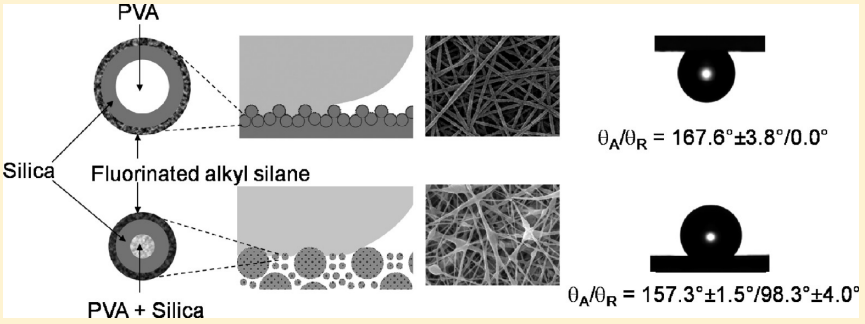

Electrospinning and silanization were synergistically employed to fabricate poly(vinyl alcohol) (PVA) and PVA/silica mixtures into flexible and chemically modifiable nanostructured surfaces with varying degrees of hydrophobicity and water adhesion. Surfaces possessing the greatest advancing water contact angle yet exhibiting a high level of water adhesion ($\theta_A/\theta_R \approx 168°/0°$) were achieved by the reaction of PVA fiber mats with multiple cycles of $SiCl_4/H_2O$ treatment, followed by silanization with (1*H*,1*H*,2*H*,2*H*-perfluorooctyl)trichlorosilane. It is postulated that the strong pinning effect and hence the water adhesion originated from the collapse of the underlying fibrous structures and the removal of air pockets. The addition of silica to the PVA matrix improved the rigidity and thus prevented the fibers from collapsing, allowing air to remain trapped within the fibrous structure and giving the surface greater water repellency. Throughout the investigation, the three wetting models—Wenzel's, Cassie–Baxter's, and the Cassie-impregnating—were regularly referred to as a conceptual framework. The hydrophobic surface that exhibited strong water adhesion, or the so-called "Petal effect", was elucidated in correlation with the fibrous structure of the film, as reviewed by microscopic analysis. In summary, electrospinning as a facile and cost-effective method provides promising opportunities for investigating the mechanistic character of nanowetting, nanoprinting, and nanocoating where the precise control of the dynamical three-phase contact line is of paramount importance.

INTRODUCTION

Wettability and the control of it are of particular academic and technological interest. The term is defined as the degree to which a specific type of liquid maintains its contact with a surface and is a consequence of both its chemical and physical attributes. Because contact angle measurements are usually performed to characterize the wettability quantitatively, the concept can be used to develop various materials that possess specific properties, such as defogging, self-cleaning, anticorrosion, and antimicrobial.[1,2] Two models that have widely been used to explain the wetting nature of a rough surface are those of Wenzel and Cassie–Baxter.[3−5] According to Wenzel's model (Figure 1a), the surface roughness increases the specific area of a surface, hence altering the wetting behavior. In some cases, the increased contact area under a complete wetting condition allows more intermolecular interactions and hence results in a larger contact angle hysteresis. In the Cassie–Baxter model (Figure 1b), the roughness allows for air to be trapped between the liquid and the underlying solid surface. Because air is hydrophobic, its presence at the liquid/solid interface helps to repel water. The decrease in the interfacial area gives rise to a reduction in the intermolecular interactions and hence a reduction in the contact angle hysteresis.

Because the interfacial phenomenon of liquid on materials of a natural origin has been a topic of intense research, another model

Received: December 16, 2010
Revised: February 17, 2011
Published: March 14, 2011

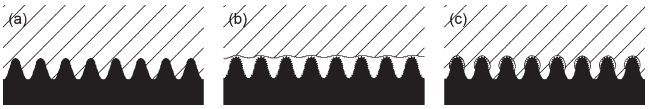

Figure 1. Schematic diagram showing the three wetting-state models: (a) Wenzel's model, (b) Cassie−Baxter's model, and (c) Cassie's impregnating wetting model.

is needed to elucidate the wetting behavior of such surfaces that exhibit water contact angles greater than 150° yet express very large contact angle hysteresis and water adhesion, such as that found on the petals of red roses (*rosea Rehd*). This phenomenon, designated as the "Petal effect" by Feng et al.,[6] is believed to be a result of the "Cassie impregnating wetting state" in which water impregnates large grooves on the petals while leaving the small grooves on the "island" dry (Figure 1c). Nonwetting over these minuscule grooves, similar to that illustrated in the Cassie−Baxter model, facilitates high advancing contact angles (θ_A), making the surface appear hydrophobic on the macroscopic level. However, the impregnation of water on the large, wettable grooves gives rise to a low receding contact angle (θ_R), resulting in high hysteresis. Whereas the contact angle hysteresis characterizes the pinning of water on a surface, the impregnation of water differentiates the "Lotus effect" from the "Petal effect". Besides red roses, Chinese kaffir lily (*Clivia miniata*) and sunflower (*Helianthus anuus*) also exhibit the same phenomenon.[6] Surfaces having this type of wetting behavior offer a great potential in specific and unique applications, such as the transport of liquid microdroplets over a surface by holding them in place without sliding or rolling and the minimization of the falling of condensed water droplets onto passengers inside an aircraft.[7−9]

Because these findings shed further light onto the structure−property relationships that govern the surface wettability on both the micro- and nanometer length scales, attempts have been made to mimic natural surface structures with synthetic materials and artificial approaches.[10−17] Many fabrication techniques have been applied as a means to modulate both the chemical and physical characteristics of these surfaces. These include laser etching, physical and/or chemical templating, and sol−gel processing.[18−21] Apart from these methods, electrospinning offers a versatile approach to fabricating unique micro- and nanostructures with interesting wetting characteristics.[11,17,22] Under the influence of a high electric field, a polymer liquid (solution or melt) is drawn out of the tip of a nozzle as a charged polymer jet, which then transforms into a minuscule fiber upon drying or solidifying and can form a nonwoven fabric on a collective target.[23] Varying degrees of wettability can be achieved by utilizing materials with a wide range of surface energies and by variation of the electrospinning conditions to tailor different surface topographies. Electrospinning has been used to fabricate various hydrophobic polymers[24−27] and inorganic silica[28−30] into fibrous substrates with suitable morphologies so as to make the surface superhydrophobic with or without subsequent chemical treatment.

Here, electrospinning and silanization are employed to fabricate nanostructured surfaces with varying degrees of hydrophobicity and water adhesion. We used poly(vinyl alcohol) (PVA), one of the most utilized hydrophilic commodity polymers, to construct flexible and chemically amendable fibrous substrates.[31−33] In particular, the inherent hydroxyl groups are prone to various chemical reactions, including but not limited to surface modification with various alkylchlorosilane reagents.[34,35] Apart from the pristine PVA solutions, mixtures of PVA and a silica sol−gel were also electrospun into fibrous substrates having different surface chemistries and topographies.[36] We discovered that, upon varying the chemical compositions and the electrospinning conditions, the hydrophobicity and water adhesion of these fibrous structures can be facilely adjusted.

EXPERIMENTAL SECTION

Materials. PVA powder (M_w = 89−98 kDa, 98−99% hydrolyzed content), silicon tetrachloride ($SiCl_4$), and (1*H*,1*H*,2*H*,2*H*-perfluorooctyl)trichlorosilane (PFOTS) were purchased from Sigma-Aldrich (USA). Tetraethylorthosilicate (TEOS) and dimethyldichlorosilane (DDS) were purchased from Fluka (USA). Toluene, ethanol, and concentrated hydrochloric acid [HCl(conc)] were obtained from Merck (Germany). All reagents were AR grade and used as received.

Preparation of Electrospun PVA and PVA/Silica Fiber Mats. A measured amount (5 g) of PVA powder was added to a 250 mL round-bottomed flask a priori filled with 50 mL of deionized water. After the contents of the flask were stirred at 80 °C for 3 h, a clear 10% (w/v) PVA solution was obtained. In a separate round-bottomed flask, TEOS and deionized water were mixed together at a 1:1 (w/w) ratio. After the pH of the solution was adjusted to 1 with HCl(conc), the TEOS solution was stirred for 1 h. The hydrolyzed TEOS and the PVA solution were then mixed to give different ratios (set as final TEOS and thus PVA at concentrations of 14.3−25% (w/v) and 7.1−5% (w/v), respectively) prior to electrospinning.

Each of the as-prepared solutions was loaded into a 10 mL syringe. A 1.5-cm-long, 20-gauge flat-tipped stainless-steel needle (i.e., outside diameter = 0.91 mm) was used as a nozzle. A syringe dosing pump (ProServe, model QIS-NE1000, The Netherlands) was used to control the flow rate of the solution. An aluminum sheet was utilized as a grounded-target plate collector. A high dc potential across the needle (connected to the positive emitting electrode) and the collector (connected to the grounding electrode) was generated from a power supply (Gamma High Voltage Research, model ES30P, USA). The applied voltages were fixed at 15 and 20 kV for PVA and PVA/TEOS solutions, respectively, and the distance between the tip of the needle and the collector was kept at 15 cm. The feed rates were preset at 1 and 3 mL/h for PVA and PVA/TEOS solutions, respectively. The collection time was fixed at 5 h. Prior to further characterization, the electrospun fiber mats were held at 95 °C under reduced pressure for 24 h to ensure the complete drying of the obtained fibrous samples.

Preparation of PVA-Silanol and PVA/Silica-Silanol Fiber Mats. The electrospun fiber mats were first dried in a Schlenk flask under reduced pressure for 2 h and subsequently purged with N_2(g). The mats were then exposed to $SiCl_4$(g) (vapor pressure = 25.9 kPa at 20 °C) via a cannula that was connected between the reaction flask and the $SiCl_4$ reservoir under a steady stream of N_2(g) at ambient temperature for 15 min. The residual $SiCl_4$ vapor was then flushed away with N_2(g) before the fiber mats were exposed to air (ca. 70% RH) for 5 min to allow the hydrolysis reaction to commence.[31] Prior to the following cycle, the sample flask was returned to a reduced pressure and purged with dry N_2(g) again.

Vapor-Phase Silanization of PVA-Silanol and PVA/Silica-Silanol Fiber Mats with Alkylchlorosilanes. In a Schlenk flask containing 0.5 mL of an alkylchlorosilane, a dried fiber mat (1 cm × 1 cm) was suspended using a sample holder, ensuring that there was no direct contact between the liquid silane and the fiber mat during the reaction. Silanization was carried out at 70 and 120 °C for DDS and PFOTS, respectively. The modified fiber mats were sequentially rinsed twice with 10 mL each of toluene, ethanol, ethanol−water (1:1 (v/v)),

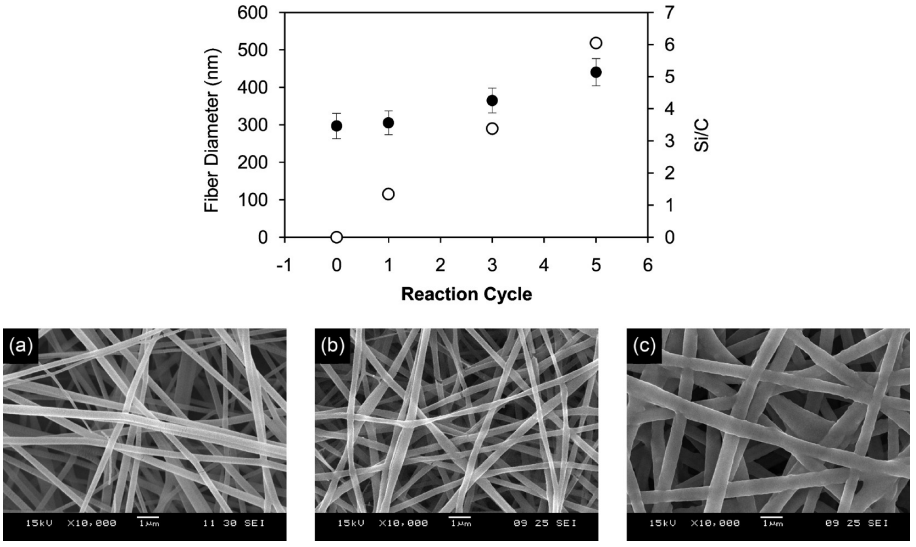

Figure 2. Diameters of individual fibers (●) and Si/C ratios (○) of the PVA fiber mats as a function of the number of $SiCl_4/H_2O$ treatment cycles (upper panel). Data are shown as the mean ± SD and are derived from 30 repetitions. (a) Representative SEM images (all at 10 000× magnification) of the PVA fiber mats (a) before and after treatment with (b) one and (c) three cycles of $SiCl_4/H_2O$ (lower panel). The micrographs shown are representative of at least five such fields of view per sample and three samples.

and water and then dried in an oven at 120 °C for 10 min. The mats were then kept in a sealed flask prior to further characterization.

Contact Angle Measurements. A contact angle goniometer, equipped with a Gilmont syringe and a 24 gauge flat-tipped needle (Ramé-Hart, model 200-F1, USA), was used to determine the water contact angles at ambient temperature. A droplet of water was placed on the surface of a fiber mat sample by bringing the mat surface into contact with the sessile droplet of water suspended at the tip of the needle. A silhouette image of the droplet was projected onto a back screen, from which the contact angle at the solid/liquid/air interface was determined. Dynamic advancing (θ_A) and receding contact angles (θ_R) were recorded while a small amount of water was either added to or withdrawn from the droplet. For the advancing measurement, the volume of the droplet was changed from 1 to 3 μL, and for the receding counterpart, it was the opposite. Both the advancing and the receding contact angles were determined when the volume of the droplet approached 2 μL. The data for each sample was taken from five different areas of the mat and analyzed by DROPimage standard 2.0, after which they were expressed as the arithmetic mean value ± standard deviation (SD).

Attenuated Total Reflectance-Fourier Transform Infrared Spectroscopy (ATR-FTIR). All spectra were collected using an FT-IR spectrometer (Thermo Scientific, model Nicolet 6700, USA) equipped with a mercury−cadmium−telluride (MCT) detector at a resolution of 4 cm^{-1} for 64 scans. The instrument was connected to a Constiuμm infrared microscope with a 15× Cassegrain infrared objective, a 10× glass objective, and a homemade slide-on germanium μIRE.

Scanning Electron Microscopy (SEM). Morphologies of the electrospun fibers, both before and after chemical modification, were investigated using a scanning electron microscope (SEM, JEOL, model JSM-6480LV, Japan). Each fiber mat sample, a priori affixed to a sample holder with a piece of adhesive tape, was coated with a thin layer of gold. The SEM images were obtained at magnifications of 3000, 5000 and 10 000×. The average diameters of the individual fibers were obtained using the Semafore software. In the case of beaded fibers, only the diameters of the fiber segments between adjacent beads were measured. Atomic compositions of the fiber mats were examined with the energy dispersive spectroscopy (EDS) capability of the SEM equipment.

Thermogravimetric Analysis (TGA). The thermal degradation behavior of all of the obtained fiber mat samples and the weight ratio of silica in the PVA-silica fiber mats were investigated by thermogravimetric analysis (TGA) (Mettler Toledo, model TGA/SDTA 851, USA) over a temperature range of 30−600 °C at a heating rate of 20 °C/min under ambient conditions.

Transmission Electron Microscopy (TEM). Internal morphologies of individual fiber segments of the electrospun fiber mats were investigated using a transmission electron microscope (TEM, JEOL model JEM-2010, Japan). The TEM images were obtained at an acceleration voltage of 200 kV at a magnification of 4000 or 10 000×.

Atomic Force Microscopy (AFM). The pore dimensions and physical strength of the electrospun fiber mats were evaluated using an atomic force microscope (AFM, Seiko model SPI 4000 Probe Station, Japan). The experiment was performed in tapping mode using a NSG 20 cantilever with a 190−325 kHz resonance frequency over 15 μm. All images were recorded in air at room temperature at a scan speed of 0.8 Hz.

RESULTS AND DISCUSSION

Preparation of PVA-Silanol Fiber Mats. Whereas the electrospinning of PVA has been heavily explored by a large number of research groups, the conditions applied in this study followed those previously described by Chuangchote and Supaphol.[33] Above a 10% (w/v) PVA concentration, bead-free fibers were formed upon electrospinning with mean fiber segment diameters of 297 ± 34 nm and a water contact angle, as measured on the surface of the fiber mat, of 52.3 ± 1.2°. To maintain the physical integrity of the PVA fibers during silanization, the fiber mats were exposed to $SiCl_4$(g) and then atmospheric moisture for up to five cycles to develop layers of silica on the surface of the individual fibers, yielding PVA-silanol fiber mats.[35] As shown in the representative SEM images (Figure 2), the resulting fibers were smooth. The Si/C ratio, as analyzed by SEM-EDS, increased linearly with the number of $SiCl_4/H_2O$ treatment cycles (within the tested range of zero to five cycles), whereas the increase in the

dx.doi.org/10.1021/la104978e |*Langmuir* 2011, 27, 3654–3661

fiber diameters was not observed until the third treatment cycle (Figure 2). This implied not only that silica coated the surface of the individual fibers but also that it infiltrated the mass of PVA fibers, presumably during the exposure cycles to $SiCl_4$ vapor in the reaction chamber prior to being exposed to atmospheric moisture. The introduction of silica layers following multiple cycles of $SiCl_4/H_2O$ treatment also resulted in a dramatic reduction in water contact angles down to 0°, rendering the obtained fiber mats superhydrophilic.

The results of the ATR-FTIR analysis (Figure 3) were additional evidence confirming the presence of silica within the PVA-silanol fiber mats. A characteristic absorption peak at 1100 cm^{-1}, corresponding to the C−O stretching of hydroxyl groups, was observed on the spectrum of the PVA fiber mat (Figure 3a). Upon exposure to multiple cycles of $SiCl_4/H_2O$ treatment, the peaks associated with the Si−O−Si/Si−O−C and the Si−OH stretching appearing at 1080 and 960 cm^{-1}, respectively, became dominant signals. This clearly confirmed the presence of silica as well as the silanol group functionality on the surface of the PVA-silanol fiber mats (Figure 3b).

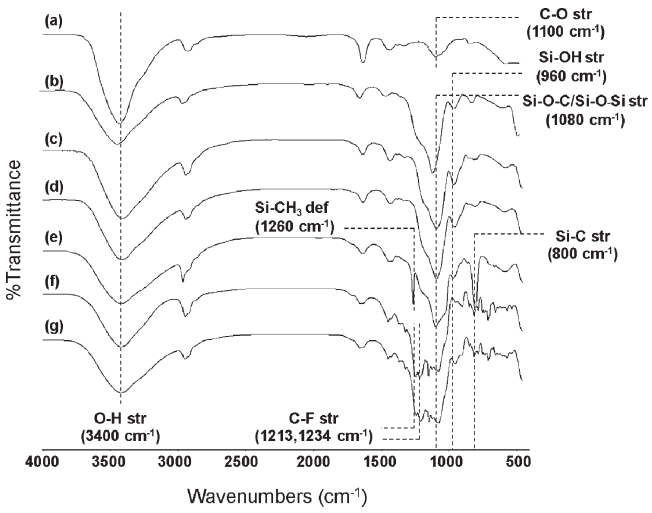

Figure 3. ATR-FTIR spectra of (a) the PVA fiber mat, (b) the PVA-silanol fiber mat, (c) the PVA/silica fiber mat, (d) the PVA/silica-silanol fiber mat, (e) the PVA/silica-silanol fiber mat after silanization with DDS, (f) the PVA-silanol fiber mat after silanization with PFOTS, and (g) the PVA/silica-silanol fiber mat after silanization with PFOTS.

Preparation of PVA/Silica and PVA/Silica-Silanol Fiber Mats. A series of PVA/TEOS solutions with TEOS concentration ranging from 14.3 to 25.0% (w/v) were electrospun into PVA/silica fiber mats of varying silica content (42−61 wt %, TGA). The morphologies and diameters of the obtained fibers as a function of the silica content in the PVA/silica fiber mats are shown in Figure 4. Upon incorporating silica into the fibers via the sol−gel process, the morphology of the fibers changed drastically from the bead-free fibers found in the PVA fiber mats (Figure 2) to the beaded fibers found in the PVA/silica fiber mats (Figure 4). Increasing the silica content decreased the diameters of the fibers between beads and increased both the bead density and the bead-to-fiber ratio. Bead formation can be ascribed to the final PVA concentration being lower (7.1, 6.3, and 5 wt %) than the original concentration of 10 wt % upon mixing with the TEOS solution prior to electrospinning. Indeed, PVA concentrations in the mixed solution of 7.1, 6.3, and 5.0 wt % yielded PVA silica fiber mats with silica contents of 42, 50, and 61%, respectively. It was hypothesized that the phase separation of the silica-rich domain, which in itself was not electrospinnable, from the PVA-rich domain played a significant role in bead formation. The θ_A values of all of the PVA/silica fiber mats were significantly (1.4- to 2.1-fold) lower than that of the original PVA fiber mat (52.3 ± 1.2°), and the fibers with the greatest silica content (Figure 4) exhibited the lowest value. However, the θ_R values of all of the PVA/silica fiber mats remained at 0°. The decreased

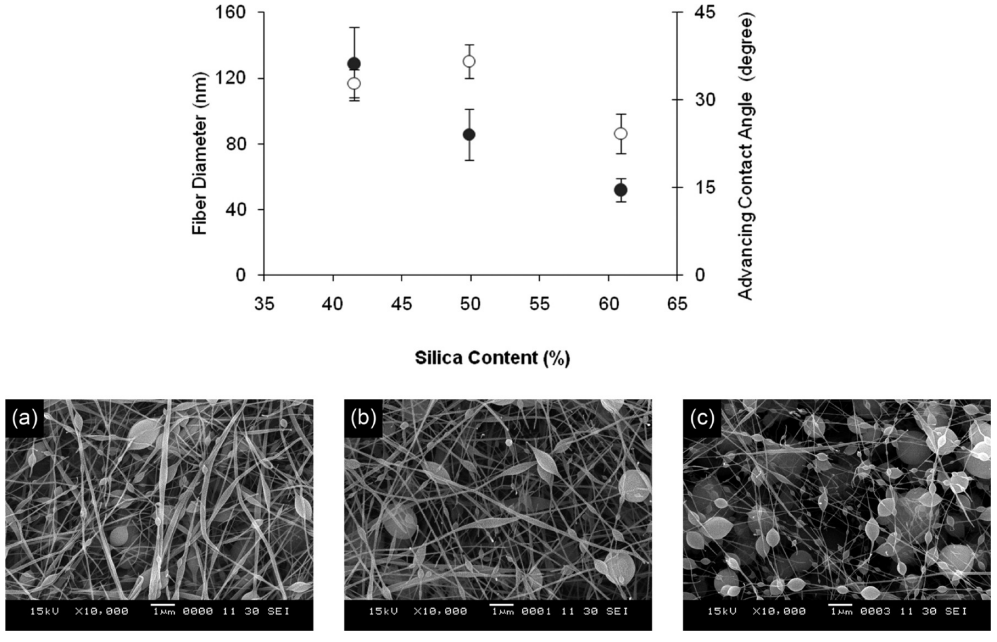

Figure 4. Diameters of individual fibers (●) and advancing water contact angles, θ_A (○), of the PVA/silica fiber mats as a function of the silica content (upper panel). Data are shown as the mean ± SD and are derived from 30 repetitions. Representative SEM images (all at 10 000× magnification) of the PVA/silica fiber mats having silica contents of (a) 42, (b) 50, and (c) 61 wt % (lower panel). The micrographs shown are representative of at least five such fields of view per sample and three samples.

dx.doi.org/10.1021/la104978e |*Langmuir* 2011, 27, 3654–3661

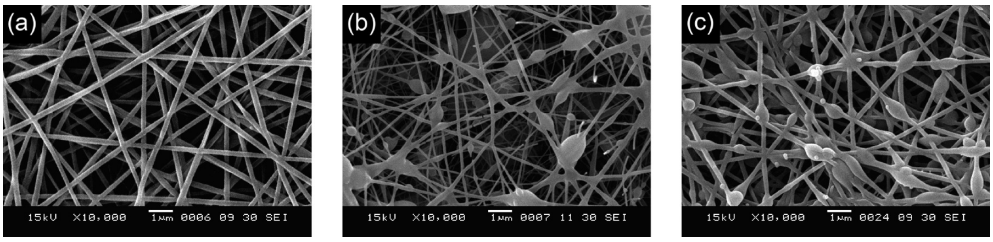

Figure 5. Representative SEM images (all at 10 000× magnification) of (a) the PVA-silanol fiber mat (electrospun from a 10% (w/v) PVA solution), (b) the PVA/silica-silanol fiber mat with a silica content of 42 wt %, and (c) the PVA-silanol fiber mat (electrospun from an 8% (w/v) PVA solution) after silanization with DDS for 4 h. The micrographs shown are representative of at least five such fields of view per sample and three samples.

contact angle is thus a result of the inclusion of the hydrophilic silica. The subsequent treatment of the PVA/silica fiber mat with three cycles of $SiCl_4/H_2O$ treatment led to the formation of the superhydrophilic PVA/silica-silanol fiber mat with a water contact angle of essentially 0°.

The fact that the same set of characteristic peaks (i.e., the Si−O−Si/Si−O−C and Si−OH stretching) was also observed for both the PVA/silica (Figure 3c) and the PVA/silica-silanol fiber mats (Figure 3d), as compared to the PVA-silanol fiber mats, implied that all of them contained similar chemical compositions, despite their different preparation methods. It also implied that the multiple-cycle $SiCl_4/H_2O$ treatment did not change the chemical functionalities of the PVA-silica fiber mats.

Silanization of PVA-Silanol and PVA/Silica-Silanol Fiber Mats. In the case of the PVA-silanol fiber mats, θ_A increased sharply from 0° to reach a maximum value of 150.6 ± 1.4° after silanization with DDS for 4 h. However, θ_R remained at 0° and showed no sign of change upon prolonged reaction. Therefore, the sole increase in θ_A gave rise to a very high contact angle hysteresis. In addition to the change in the wettability, the fiber diameters also decreased from 365 ± 33 nm for the PVA-silanol fiber mats that had been exposed to three cycles of $SiCl_4/H_2O$ treatment to 213 ± 19 nm upon silanization with DDS (Figure 5a). The collapse of the soft PVA core due to the cross-linking of the silica shell by DDS was postulated to be the cause of the observed decrease in the fiber diameters. In contrast, the diameter of the PVA/silica-silanol fibers did not significantly change after silanization with DDS (Figure 5b): e.g., the mean fiber diameters of 129 ± 22 nm being observed for the PVA/silica (42 wt %) fiber mat that had been exposed to three cycles of $SiCl_4/H_2O$ treatment and 141 ± 33 nm after a 4 h reaction with DDS. This is likely a result of the increase in the rigidity of the fibers in response to the presence of silica within the PVA/silica-silanol fibers. As illustrated in Figure 3e, the successful silanization of the PVA/silica-silanol fiber mats by DDS was confirmed by the presence of the signals of Si-CH_3 deformation at 1260 cm^{-1} and Si−C stretching at 800 cm^{-1}. The same set of signals was also observed for the PVA-silanol fiber mats after silanization with DDS (data not shown).

The difference between the PVA-silanol and PVA/silica-silanol fiber mats upon silanization was seen not only in their morphologies but also in their wettability. Although the PVA-silanol fiber mats did not display a measurable θ_R even after a prolonged reaction time of up to 8 h, the PVA/silica-silanol fiber mats began to show increased θ_R values after only 2 h of reaction, and the contact angles reached maximal values of 151.4°/83.3° after 4 h of reaction. In light of Wenzel's model, it was hypothesized that the beads enhanced the apparent roughness of the PVA/silica-silanol surface. To address this issue, another

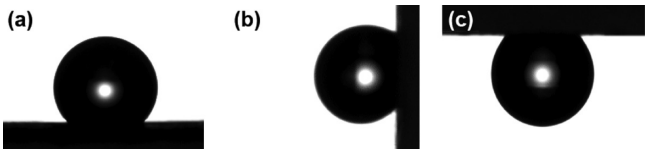

Figure 6. A 2 μL water droplet on a PVA-silanol fiber mat after silanization with PFOTS orientated in the (a) horizontal, (b) vertical, and (c) inverted positions. The photographs shown are representative of at least five such trials on three different samples.

set of PVA-silanol fiber mats was fabricated from an 8% (w/v) PVA solution, the concentration of which is known to yield beaded fibers,[33] followed by treatment with three $SiCl_4/H_2O$ cycles. Interestingly, the θ_A of these PVA-silanol fiber mats after silanization with DDS (Figure 5c) reached a maximum value of 142.1 ± 1.8° and θ_R remained at 0°. Thus, the presence of beads is not the only reason for the observed difference in the wetting behavior between the silanized PVA-silanol and the PVA/silica-silanol fibers.

The physical characteristics of the individual fibers formed by electrospinning might not be the sole influencing parameter governing the pinning of the three-phase contact line. Rather, it was hypothesized that the pinning behavior could be reduced by an increase in θ_R. To evaluate this notion, the more hydrophobic silane, PFOTS, was used instead of DDS. As expected, a greater extent of fiber contraction upon reaction with PFOTS was observed in case of the PVA-silanol fiber mats (365 ± 33 to 196 ± 18 nm) as opposed to the PVA/silica-silanol fiber mats (129 ± 22 to 132 ± 15 nm). Both types of fiber mats exhibited the same characteristic ATR-FTIR peaks at 1213 and 1234 cm^{-1}, corresponding to the C−F stretching of the perfluorooctyl groups (Figure 3f,g). In addition, it should be emphasized that the type of the silane used had no noticeable impact on the morphology of the silanized fibers. As a consequence of the perfluorooctyl moiety from PFOTS, the θ_A/θ_R of the silanized PVA/silica-silanol fiber mats increased to 157.3 ± 1.5°/98.3 ± 4.0°. Despite their very high θ_A (167.6 ± 3.8°), the silanized PVA-silanol fiber mats still exhibited a θ_R of 0°. The strong water adhesion of these particular fiber mats having a contact angle hysteresis of as high as ∼168° is shown in Figure 6, where the water droplet (2 μL) remained intact on the PVA-silanol fiber mat that had been silanized by PFOTS and no sliding of the droplet was discernible even in the vertical and inverted positions. To this end, it seems that neither the physical attributes (i.e., the formation of beaded fibers as submitted by the electrospinning condition) nor the chemical contribution from PFOTS can account for the difference in the wetting behavior between the PVA-silanol and PVA/silica-silanol fiber mats.

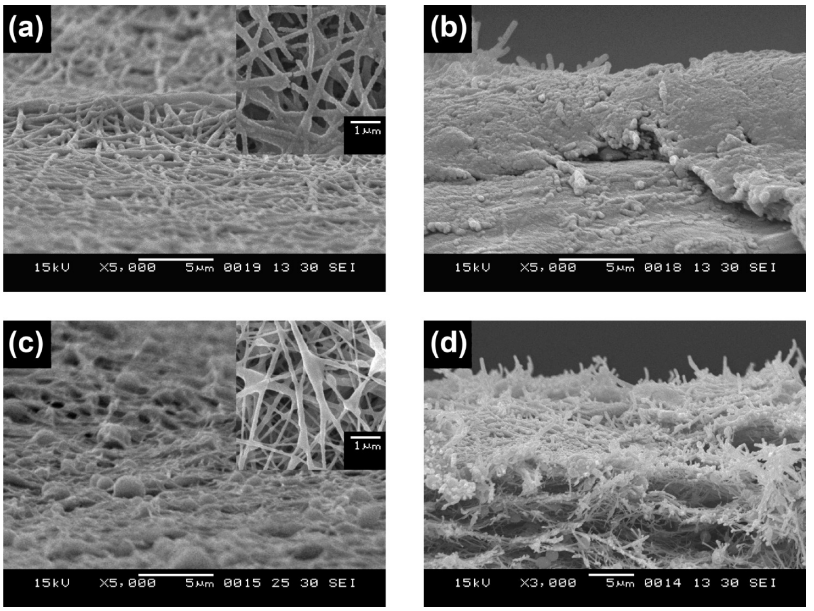

Figure 7. Representative SEM images (5000× magnification for a−c and 3000× magnification for d) of the side-view and top-view (inset) morphology of the (a) PVA-silanol fiber mat and (c) PVA/silica-silanol fiber mat together with the cross-sectioned structures of the (b) PVA-silanol fiber mat and (d) the PVA/silica-silanol fiber mat after silanization with PFOTS. The micrographs shown are representative of at least five such fields of view per sample and three samples.

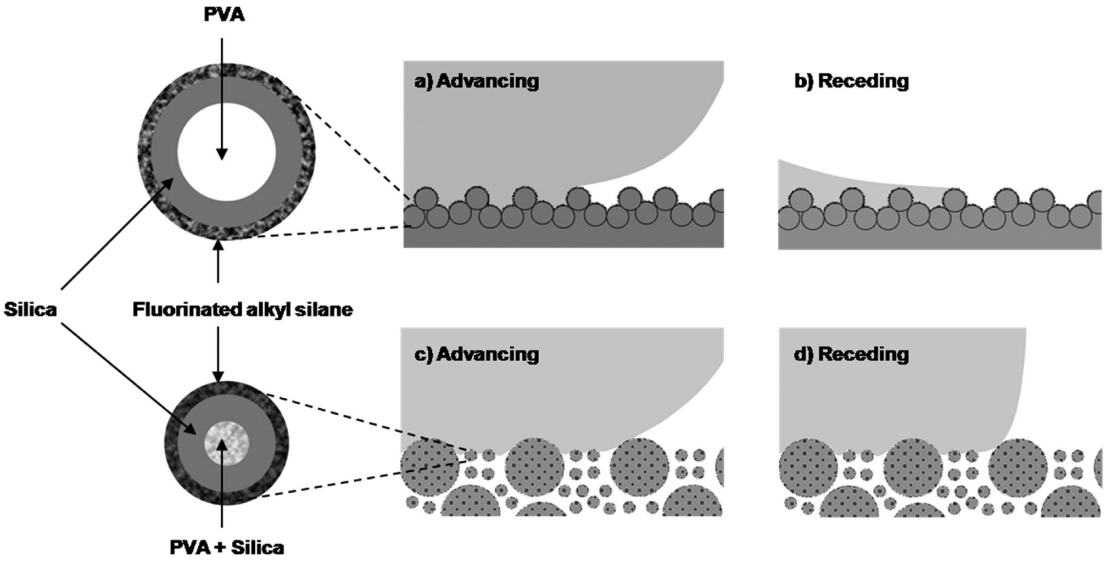

Figure 8. Schematic illustration of the proposed wetting behavior of the (a, b) PVA-silanol fiber mat and (c, d) PVA/silica-silanol fiber mat after silanization with PFOTS. With reference to the Cassie impregnating wetting model, the underlying dense layer in a and b accounts for the physical origin of the strong pinning in the PVA-silanol fiber mat. In light of Wenzel's model, the presence of hydrophobic air pockets (white regions in c and d) helped increase the receding contact angles of the PVA/silica-silanol fiber mat.

Undeniably, the high advancing contact angles and strong water adhesion of the silanized PVA-silanol fiber mats resembled those of the Petal effect, as previously mentioned. Alternatively, the microstructures of these mats could be the physical origin of the wettability variation. Cross-section, top-view, and side-view SEM micrographs of the silanized PVA-silanol and the PVA/silica-silanol fiber mats revealed that the physical appearance of the underlying structure between these two types of fiber mats was distinctively different (Figure 7). Appearing fibrous on the surface, the PVA-silanol fiber mat bore a single dense layer with the fibers completely merged and collapsed underneath (Figure 7a,b). This underlying, featureless layer relegated the ability of the mat to hold hydrophobic air pockets on the surface, resulting in a highly water impregnable surface. As illustrated in the schematic representation of the proposed model (Figure 8a), water protrusion into the spacing between the fiber bundles down to the flat layer underneath mirrored that of the wettable large groove in the Petal effect. In reference to the Cassie impregnating wetting model, this underlying dense layer consequently accounted for the physical origin of the strong pinning of a

dx.doi.org/10.1021/la104978e |*Langmuir* 2011, 27, 3654–3661

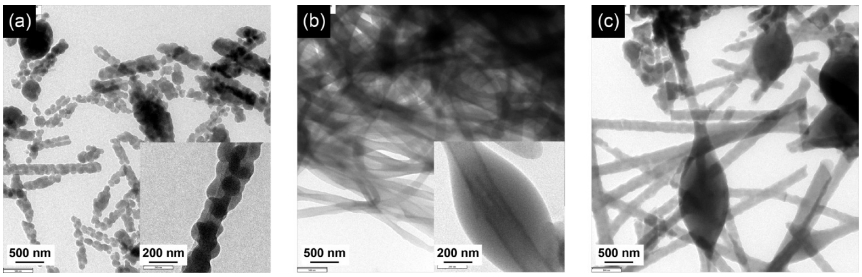

Figure 9. Representative TEM images of (a) the PVA/silica-silanol fiber mat and both (b) the PVA-silanol fiber mat and (c) the PVA/silica-silanol fiber mat after silanization with PFOTS. The micrographs shown are representative of at least five such fields of view per sample and three samples.

water droplet on this type of fiber mat (Figure 8b). In contrast, the inner structure of the PVA/silica-silanol fiber mats remained fibrous, with their minuscule air pockets among the fibers being firmly intact (Figures 7c,d). In light of Wenzel's model (Figure 8c), the presence of these hydrophobic air pockets differentiates the receding behavior of the PVA-silanol fiber mat (Figures 8b) from that of the PVA/silica-silanol fiber mat (Figures 8d).

The proposed internal structures of the electrospun fiber mats as depicted in Figure 8 were confirmed by TEM analysis. As can be seen in Figure 9a, discrete silica particles are dispersed within the PVA matrix throughout the length of PVA/silica-silanol individual fibers as previously anticipated. Such phase separation can no longer be detected after the fiber mat is subjected to silanization by PFOTS (Figure 9c). Its morphology is not distinguishable from that of the PFOTS-silanized PVA-silanol fiber mat (Figure 9b). This evidence strongly suggests that the layer of silanized PFOTS can well cover the fiber mats in both cases. Interestingly, the image shown in the inset of Figure 9b clearly demonstrated that there was an inorganic coating layer on the PVA fiber.

To determine the pore/groove size of the fiber mats, AFM analysis was conducted on both the PVA-silanol and the PVA/silica-silanol fiber mats. It was found that both types of fiber mats exhibited an average pore/groove size of $2 + 0.5\ \mu$m. Thus, the speculation that the variation in contact angle hysteresis may originate from the different groove size can be ruled out. In fact, the similar petal-like characteristic has been previously reported on the electrospun titania fiber mats of which pore dimensions were in a similar range[11] despite the fact that the reported value of the pore/groove size is much smaller than that generated by templates as reported by Feng et al.[6]

It should be emphasized that the fibrous structure generated in this research was aimed to be used in the form of a coating layer, not as a free-standing film. The fact that the thin layer of all of the fiber mats supported on aluminum sheets, used as the collective target during electrospinning, could withstand mechanical distortion by bending and showed no sign of breakage could be used as practical evidence of their flexibility. Taking advantage of the AFM analysis used for the determination of the pore/groove size, the nanoscopic indentation test was also performed to estimate individual fiber strength. The returned forces for the PFOTS-silanized PVA-silanol fiber and the PVA/silica-silanol fiber were 186 ± 32 and 149 ± 18 nN, respectively, thereby implying their comparable physical strength.

To this end, this work has demonstrated that relatively flexible surfaces having a petal-like wetting characteristic can be fabricated by electrospinning from economically available PVA in combination with surface silanization without the requirement for microstructured templates. This simple, versatile method should make the application of these surfaces more commercially accessible.

CONCLUSIONS

Electrospinning has been successfully applied to fabricate fiber mats with unique morphologies and varying degrees of wettability. A superhydrophobic surface with a high water adhesion was achieved by the reaction of PVA fiber mats with multiple cycles of $SiCl_4/H_2O$ treatment followed by silanization with PFOTS. Strong pinning and thus water adhesion originated from the collapse of the underlying fibrous structures, removing the air pockets between the water and surface of the fiber mats. The addition of silica improved the fibers' rigidity and prevented the collapse, allowing air to be trapped and making the surfaces more water-repellent. The control of wettability with such a facile, cost-effective approach offers the possibility for further exploration of this nanofabrication method for applications in nanowetting, nanoprinting, and nanocoating.

AUTHOR INFORMATION

Corresponding Author

*Tel: +66-2218-7627 ext 102. Fax: +66-2218-7598. E-mail: vipavee.p@chula.ac.th.

ACKNOWLEDGMENT

Financial support of this work by the Young Scientist and Technologist Program (YSTP), sponsored by the National Science and Technology Development Agency (NSTDA), Thailand, awarded to T.P., N.I., and V.P.H., and by the Organic Synthesis Research Unit (the Ratchadapiseksompoj Endowment Fund, Chulalongkorn University) is acknowledged. We are grateful for the language editing service provided by Dr. Robert Butcher, the Publication Counselling Unit (PCU), Faculty of Science, Chulalongkorn University.

REFERENCES

(1) Fujishima, A.; Rao, T. N.; Tryk, D. A. *J. Photochem. Photobiol., C* **2000**, *1*, 1–21.
(2) Guo, Z. G.; Zhou, F.; Hao, J. C.; Liu, W. M. *J. Am. Chem. Soc.* **2005**, *127*, 15670–15671.
(3) Wenzel, R. N. *Ind. Eng. Chem.* **1936**, *28*, 988–994.
(4) Cassie, A. B. D.; Baxter, S. *Trans. Faraday Soc.* **1944**, *3*, 546–551.
(5) Johnson, R. E.; Dettre, R. H. *Adv. Chem. Ser.* **1964**, *43*, 112–135.
(6) Feng, L.; Zhang, Y.; Xi, J.; Zhu, Y.; Wang, N.; Xia, F.; Jiang, L. *Langmuir* **2008**, *24*, 4114–4119.

(7) Jin, M.; Feng, X.; Feng, L.; Sun, T.; Zhai, J.; Li, T.; Jiang, L. *Adv. Mater.* **2005**, *17*, 1977–1981.
(8) Hong, X.; Gao, X.; Jiang, L. *J. Am. Chem. Soc.* **2007**, *129*, 1478–1479.
(9) Bhushan, B.; Her, E. K. *Langmuir* **2010**, *26*, 8207–8217.
(10) Li, Y. B.; Zheng, M. J.; Ma, L.; Zhong, M.; Shen, W. Z. *Inorg. Chem.* **2008**, *47*, 3140–3143.
(11) Tang, H. Z.; Wang, H.; He, J. H. *J. Phys. Chem. C* **2009**, *113*, 14220–14224.
(12) Song, X. Y.; Zhai, J.; Wang, Y. L.; Jiang, L. *J. Phys. Chem. B* **2005**, *109*, 4048–4052.
(13) Balu, B.; Breedveld, V.; Hess, D. W. *Langmuir* **2008**, *24*, 4785–4790.
(14) Lai, Y. K; Lin, C. J.; Huang, J. Y.; Zhuang, H. F.; Sun, L.; Nguyen, T. *Langmuir* **2008**, *24*, 3867–3873.
(15) Winkleman, A.; Gotesman, G.; Yoffe, A.; Naaman, R. *Nano Lett.* **2008**, *8*, 1241–1245.
(16) Bliznakov, S.; Liu, Y.; Dimitrov, N. *Langmuir* **2009**, *25*, 4760–4766.
(17) Sharma, C. S.; Vasita, R.; Upadhyay, D. K.; Sharma, A.; Katti, D. S.; Venkataraghavan, R. *Ind. Eng. Chem. Res.* **2010**, *49*, 2731–2739.
(18) Gao, X. F.; Yao, X.; Jiang, L. *Langmuir* **2007**, *23*, 4886–4891.
(19) Li, Y.; Jia, W. Z.; Song, Y. Y.; Xia, X. H. *Chem. Mater.* **2007**, *19*, 5758–5764.
(20) Shang, H. M.; Wang, Y.; Limmer, S. J.; Chou, T. P.; Takahashi, K.; Cao, G. Z. *Thin Solid Films* **2005**, *472*, 37–43.
(21) Bormashenko, E.; Stein, T.; Pogreb, R.; Aurbach, D. *J. Phys. Chem. C* **2009**, *113*, 5568–5572.
(22) Wang, L. F.; Zhao, Y.; Wang, J. M.; Hong, X.; Zhai, J.; Jiang, L.; Wang, F. S. *Appl. Surf. Sci.* **2009**, *255*, 4944–4949.
(23) Guptaa, P.; Elkins, C.; Long, T. E.; Wilkes, G. L. *Polymer* **2005**, *46*, 4799–4810.
(24) Ma, M.; Hill, R.; Lowery, J.; Fridrikh, S.; Rutledge, G. *Langmuir* **2005**, *21*, 5549–5554.
(25) Ma, M.; Mao, Y.; Gupta, M.; Gleason, K.; Rutledge, G. *Macromolecules* **2005**, *38*, 9742–9748.
(26) Crick, C. R.; Parkin, I. P. *Thin Solid Films* **2010**, *518*, 4328–4335.
(27) Harton, S. E.; Templeman, C. G.; Vyletel, B. *Macromolecules* **2010**, *43*, 3173–3176.
(28) Shang, H. M.; Wang, Y.; Takahashi, K.; Cao, G. Z. *J. Mater. Sci.* **2005**, *40*, 3587–3591.
(29) Latthe, S. S.; Imai, H.; Ganesan, V.; Rao, A. V. *Microporous Mesoporous Mater.* **2010**, *130*, 115–121.
(30) Rao, A. V.; Latthe, S. S.; Nadargi, D. Y.; Hirashima, H.; Ganesan, V. *J. Colloid Interface Sci.* **2009**, *332*, 484–490.
(31) Koski, A.; Yim, K.; Shivkumar., S. *Mater. Lett.* **2004**, *58*, 493–497.
(32) Son, W. K.; Youk, J. H.; Lee, T. S.; Park, W. H. *Mater. Lett.* **2005**, *59*, 1571–1575.
(33) Chuangchote, S.; Supaphol, P. *J. Appl. Polym. Sci.* **2008**, *108* (2), 969–978.
(34) Nishino, T.; Meguro, M.; Nakamae, K. *Int. J. Adhes. Adhes.* **1999**, *19*, 399–403.
(35) Quarmyne, M.; Chen, W. *Langmuir* **2003**, *19*, 2533–2535.
(36) Shao, C.; Kim, H. Y.; Gong, J.; Ding, B.; Lee, D. R.; Park, S. J. *Mater. Lett.* **2003**, *57*, 1579–1584.